

**Boosted Higgses from chromomagnetic  $b$ 's:  $b\bar{b}h$  at high luminosity**Joseph Bramante<sup>a,1</sup> Antonio Delgado<sup>b,1,2</sup> Landon Lehman<sup>c,1</sup> and Adam Martin<sup>d1</sup><sup>1</sup>*Department of Physics, University of Notre Dame,  
225 Newland Hall, Notre Dame, IN, USA, 46556*<sup>2</sup>*PH-TH Department, CERN, CH-1211, Geneva 23, Switzerland*

This paper examines detection prospects and constraints on the chromomagnetic dipole operator for the bottom quark. This operator has a flavor, chirality and Lorentz structure that is distinct from other dimension six operators considered in Higgs coupling studies. Its non-standard Lorentz structure bolsters boosted  $b\bar{b}h$  events, providing a rate independent signal of new physics. To date, we find this operator is unconstrained by  $pp \rightarrow h + \text{jets}$  and  $pp \rightarrow b\bar{b}$  searches: for order-one couplings the permitted cutoff  $\Lambda$  for this operator can be as low as  $\Lambda \sim 1$  TeV. We show how to improve this bound with collider cuts that allow a  $b$ -tagged Higgs plus dijet search in the Higgs to diphoton decay channel to exclude cutoffs as high as  $\sim 6$  TeV at  $2\sigma$  with  $3 \text{ ab}^{-1}$  of luminosity at the 14 TeV LHC. Cuts on the  $p_T$  of the Higgs are key to this search, because the chromomagnetic dipole yields a non-standard fraction of boosted Higgses.

arXiv:1410.3484v1 [hep-ph] 13 Oct 2014

---

<sup>a</sup> jbraman2@nd.edu<sup>b</sup> antonio.delgado@nd.edu<sup>c</sup> llehman@nd.edu<sup>d</sup> amarti41@nd.edu

## CONTENTS

I.	Introduction	2
II.	The chromomagnetic dipole	4
	A. Boosted particles from the chromomagnetic dipole	5
	B. Quark chirality and the chromomagnetic dipole	7
	C. Other operators and general EFT remarks	8
III.	Constraints on the bottom quark chromomagnetic dipole	10
	A. $b$ -jet production; $pp(\bar{p}) \rightarrow b\bar{b}$	10
	B. Inclusive Higgs production: $pp \rightarrow h$	12
	C. Higgs plus dijets: $pp \rightarrow h + jj$	13
IV.	Press the $b$ -tag button	14
	A. Constraints on $b\bar{b}h$ at the 8 TeV LHC	14
	B. Constraints on $b\bar{b}h$ at the 14 TeV LHC	16
V.	Conclusions	17
	References	18

## I. INTRODUCTION

The bottom quark is the heaviest fundamental fermion lighter than the Higgs, the predominant decay product of the Higgs, and the most easily tagged quark at LHC energies. For these reasons, new physics contributions from effective operators with bottom quarks will be sought out as the LHC ramps to higher energies. The search is already afoot for non-standard Higgs interactions encapsulated in higher-dimensional Higgs operators [1–16]. Effective operator searches that are sensitive to a subset of possible operators are particularly important, because each independent high energy cross-section measurement of Higgs couplings provides information that complements constraints from flavor, precision electroweak, and also non-Higgs searches at the Tevatron and LHC. For certain higher dimensional operators, high energy Higgs studies will place the strongest bounds, or more optimistically, the best opportunity for discovery.

Motivated by these considerations, this article examines non-standard interactions between the Higgs and bottom quarks. Bottom quarks play the most important role in Higgs physics since  $\Gamma(h \rightarrow b\bar{b})$  is the largest partial width of the Higgs boson. Despite this, alternative Higgs-bottom dynamics are relatively unexplored. Existing work [17] that does incorporate non-Standard Model (SM)  $hb\bar{b}$  dynamics has thus far focused on SM-like (i.e. Yukawa) interactions with non-SM strength, rather than more general kinematic structures.

New physics operators can affect Higgs observables in two ways: normalization and shape. By normalization we mean that adding new physics affects the overall rate of events, but does not change any differential kinematic distributions, while a shape change means that the total event rate is unchanged but the kinematic distributions of particles shift. For example, consider the SM extended by a new physics (NP) operator

$$\mathcal{L}_1 \supset c_{SM} \mathcal{O}_{SM} + c_{NP} \mathcal{O}_{NP}. \tag{1}$$

If the Lorentz or chirality structure and field content of the two operators is the same, the NP effects can be recast as a change in the SM coefficient:  $c_{SM} \rightarrow c_{SM} + f(c_{NP})$ . In this case, all distributions will be SM-like but the total rate will change. Most Higgs constraints to date have focused on this possibility. However, if the two operators have different Lorentz structures, the NP and SM events can be distinguished by using kinematic cuts to select for non-standard distributions of final state particles.

This distinction between normalization effects and shape effects can also be phrased in terms of signal strength  $\mu^{\text{collider}}$ , defined as the ratio of Higgs events in some new physics scenario relative to the number of events in the SM. The number of events is the product of the luminosity  $\mathcal{L}$ , the production cross section  $\sigma(pp \rightarrow h + X)$  (where  $X$  is some other potential SM particle produced in association with the Higgs), the Higgs branching ratio  $BR$  into whatever final state we are observing, the analysis cut acceptance  $A$ , and the efficiency  $\epsilon$ . Throughout this article we make a distinction between the acceptance, which is the fraction of events that pass certain cuts, and the efficiency, the probability that objects satisfying the cuts are correctly captured by the experiment. Written out explicitly

$$\mu^{\text{collider}} = \frac{\mathcal{L} \sigma(pp \rightarrow h + X) BR A \epsilon}{\mathcal{L} \sigma(pp \rightarrow h + X)_{SM} BR_{SM} A_{SM} \epsilon} \quad (2)$$

The luminosity and efficiency cancel in the ratio, but the acceptance does not. The only time the acceptance cancels in the ratio is when new physics modifies the strength of the Higgs interaction, but does not change the kinematics of events, leaving acceptance unchanged; in this case, the signal strength reduces to the ratio of production cross sections times branching ratios, what we will call  $\mu^{\text{parton}}$ ,

$$\mu^{\text{parton}} = \frac{\sigma(pp \rightarrow h + X) BR}{\sigma(pp \rightarrow h + X)_{SM} BR_{SM}}. \quad (3)$$

This simplified scenario is attractive because it contains only theoretically defined quantities and is independent of the experiment. However, it only applies to a limited set of new physics scenarios. In general the acceptance must be included and the signal strength becomes a more involved and analysis-dependent quantity.

The  $b$  quark chromomagnetic dipole operator, defined in the next section and examined throughout this paper, is one example of an operator which changes both the rate and kinematic distribution of collider events which contain a Higgs boson, making it ideal for a study of new physics arising from non-standard Higgs couplings to  $b$  quarks. In this paper we explore existing constraints on and high luminosity discovery prospects for the bottom quark chromomagnetic dipole operator. While our focus will be on the Standard Model augmented with a single new physics operator, the methods and constraints herein can also be applied to more complicated scenarios involving multiple operators. Non-standard kinematic structure is not unique to the chromomagnetic  $b$ -quark operator, and several studies exist in the literature exploring how kinematic distributions can be used to pin down certain new physics effects in associated production  $pp \rightarrow W/Z + h$ , Higgs plus jet production  $pp \rightarrow h + j$ , and  $pp \rightarrow t\bar{t}h$  events [15, 18–38].

The remainder of this paper is organized as follows. In Section II, we comment on the properties and structure of the  $b$  quark chromomagnetic dipole operator  $\mathcal{O}_{ghd}$ , pointing out the kinematic and chiral properties it has which differ from the SM. Section III surveys the interactions from  $\mathcal{O}_{ghd}$  that lead to new physics contributions to  $pp \rightarrow \bar{b}bh$  and  $pp \rightarrow \bar{b}b$  at tree level, and to  $pp \rightarrow h$  at one loop level, then addresses the constraints from existing searches in each of these channels. In Section IV we discuss opportunities to explore BSM  $\bar{b}bh$  parameter space with improved searches

at both the 8 and 14 TeV LHC runs, both through  $b$ -tagging and selection of Higgs decays boosted by chromomagnetically dipolarized  $b$  quarks. We conclude in Section V with a discussion of high luminosity prospects for the bottom quark chromomagnetic dipole.

## II. THE CHROMOMAGNETIC DIPOLE

To pursue a clear example of non-standard final state kinematic morphology for  $b$  quarks and the Higgs boson, in this article we focus on the bottom quark chromomagnetic dipole operator

$$\mathcal{O}_{ghd} = \frac{c_{ghd}}{\Lambda_0^2} (Q_j^\dagger H) Y_{d,ij} \bar{\sigma}_{\mu\nu} t^A d_i^{c\dagger} G_A^{\mu\nu} + h.c. \quad (4)$$

Here  $c_{ghd}$  is the new physics coupling,  $\Lambda_0$  is the energy scale suppressing the higher-dimensional operator, and  $Y_d$  is an insertion of the down-type quark Yukawa matrix. There are a number of works that list dimension-6 operators and constrain them with Higgs measurements (see Refs. [16, 39, 40]) and much recent work studying the coupling of the Higgs to third generation quarks [38, 41–46]. However, the  $b$  quark chromomagnetic dipole has only been studied for its modification of the  $pp \rightarrow h + X$  cross-section (where  $X$  is another SM parton) [17]. Some work, both pre- and post-Higgs discovery, on the collider bounds on the top quark chromomagnetic dipole, the cousin of Eq. (4), can be found in [17, 21, 37].

By including the down-quark Yukawa matrix in Eq. (4) we have rendered this operator automatically minimally-flavor-violating, meaning the same field redefinitions that diagonalize the down-quark mass matrix also diagonalize  $\mathcal{O}_{ghd}$ . This guarantees that the  $\mathcal{O}_{ghd}$  operator does not induce new flavor-violating interactions (at least at tree-level), which are tightly constrained by flavor physics [47]. Diagonalized,  $\mathcal{O}_{ghd}$  contains chromomagnetic dipole interactions for the down and strange quarks, as well as for the bottom. However, as the down and strange interactions are suppressed by their corresponding tiny Yukawa couplings, we will forget about them here. We will also assume that  $c_{ghd}$  is real to avoid constraints from CP-violation. Thus, Eq. (4) approximately reduces to a chromomagnetic dipole moment for the bottom quark alone

$$\mathcal{O}_{ghd} \sim \frac{c_{ghd}}{\Lambda_0^2} (Q_3^\dagger H) y_b \bar{\sigma}_{\mu\nu} t^A b^{c\dagger} G_A^{\mu\nu} + h.c. \quad (5)$$

Our main interest in this paper is the constraints and prospects for the operator in Eq. (5), however there are multiple ways that we can express its strength. One possibility is to combine the  $y_b$  factor, coefficient  $c_{ghd}$  and  $\Lambda_0$  all into an ‘effective cutoff’  $\Lambda_{\text{eff}}$ , which we can adjust. Another possibility is to fix  $\Lambda_0$  to some value, then separately dial  $c_{ghd}$ . Within the effective theory, this difference in presentation is purely aesthetic. The convention we will use throughout this paper is to fix the combination

$$\frac{y_b}{\Lambda_0^2} \equiv \frac{1}{\Lambda^2} = \frac{1}{(6 \text{ TeV})^2} \quad (6)$$

then vary  $c_{ghd}$  to adjust the strength of  $\mathcal{O}_{ghd}$ . We choose this convention for two reasons: i.) for  $\Lambda_0 = 1 \text{ TeV}$ , the same value we used when studying the chromomagnetic top quark operator in Ref. [37]<sup>1</sup>, the combination  $y_b/\Lambda_0^2 \sim 1/(6 \text{ TeV})^2$ , and ii.) the highest dijet invariant masses currently probed by the LHC are  $\sim 6 \text{ TeV}$ . As we will see,  $\mathcal{O}_{ghd}$  contributes to  $pp \rightarrow \bar{b}b$  production, so a natural starting point for the scale suppressing  $\mathcal{O}_{ghd}$  is the highest scale probed in  $pp \rightarrow \bar{b}b$ .

<sup>1</sup> In that work, as  $y_t \cong 1$ , we did not distinguish between  $\Lambda_0$  and  $\Lambda$ .

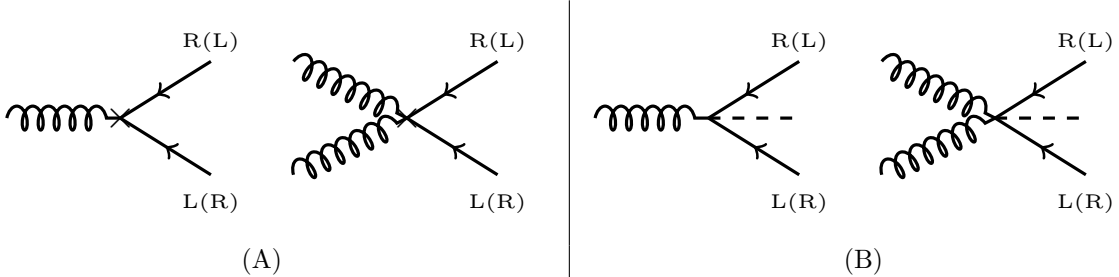


Figure 1. (A) These diagrams illustrate that the interference term between SM and chromomagnetic dipole  $b\bar{b}$  production will require a chirality flip. This flip suppresses the bottom quark chromomagnetic dipole contribution to bottom diquark production (relative to the top quark, which receives substantial corrections to  $t\bar{t}$  production from its chromomagnetic dipole) by a factor of the bottom Yukawa coupling,  $y_b$ . (B) These diagrams show  $s$ -channel  $b\bar{b}h$  processes from  $\mathcal{O}_{ghd}$ .

In addition to the ambiguities in defining the strength of  $\mathcal{O}_{ghd}$ , there are also subtleties in its interpretation, especially for  $c_{ghd} > 1$ , which we comment on in Sec. II C.

Expanding the Higgs about its vacuum expectation value,  $\mathcal{O}_{ghd}$  contains four separate interactions: a 4-point interaction involving a Higgs, gluon,  $b_L$  and  $b_R$ , a 5-point interaction with a Higgs, two gluons,  $b_L$  and  $b_R$ , a 4-point interaction involving two gluons,  $b_L$  and  $b_R$ , and a 3-point interaction between a gluon,  $b_L$  and  $b_R$ . Each of these  $n$ -point interactions introduces detectable modifications to the SM. The Feynman diagrams for these vertices are displayed in Fig. 1. All interactions involve opposite chirality  $b$  quarks, and the single gluon interactions are all proportional to the momentum carried by the gluon. These two features are the source of the kinematic difference between  $\mathcal{O}_{ghd}$  and the SM, and the subject of the next subsections.

### A. Boosted particles from the chromomagnetic dipole

The first structural feature we address is the gluon momentum dependence carried by all single-gluon interactions in  $\mathcal{O}_{ghd}$ . This feature will make the biggest impact in processes where the gluon momentum can be large, and little to no impact in processes where the gluon momentum is fixed and small. Two processes that sit in the first category are  $pp \rightarrow b\bar{b}h$  and  $pp \rightarrow b\bar{b}$ . Both contain  $s$ -channel gluon diagrams with one end of the gluon propagator terminating in the momentum-dependent  $\mathcal{O}_{ghd}$  vertex (see Fig. 2). The larger the  $\sqrt{\hat{s}}$ , or, equivalently, the larger the boost of the final state  $b, \bar{b}$  or  $h$ , the larger the effect  $\mathcal{O}_{ghd}$  has on the process. This trend can be contrasted with  $pp \rightarrow h$ , which receives a contribution from the momentum dependent  $\mathcal{O}_{ghd}$  interactions at one-loop level (see Fig. 7). In  $pp \rightarrow h$ , the characteristic momentum scale of the incoming gluons is fixed to  $O(m_h) \ll \Lambda$ , so there is no way to enhance the new physics effects by cutting events to find special corners of kinematic phase space.

To quantitatively study how the gluon momentum dependence of  $\mathcal{O}_{ghd}$  affects the kinematics in  $b\bar{b}h$  events we implemented  $\mathcal{O}_{ghd}$ , along with standard model effective couplings of the Higgs boson to gluons and photons [48–50], in FeynRules [14, 51] and generated parton level events using MadGraph5 aMC@NLO [52]. Throughout this paper, we will refer to this model as “SM +  $\mathcal{O}_{ghd}$ ”. The resulting Higgs  $p_T$  spectra in  $pp \rightarrow b\bar{b}h$  events is shown in Fig. 3 for several different values of  $c_{ghd}$ . Clearly, as  $|c_{ghd}|$  is increased, there is a trend towards more high- $p_T$  Higgs bosons, as expected from the Higgs momentum dependence of the chromomagnetic dipole operator. At the same time, the spectra from all  $c_{ghd}$  and the SM coincide at low  $p_{T,h}$ . Depending on  $c_{ghd}$ , the spectra begin to differ from the SM curve at  $p_{T,h} \sim 100 - 200$  GeV; while these  $p_{T,h}$  values are high, the center of

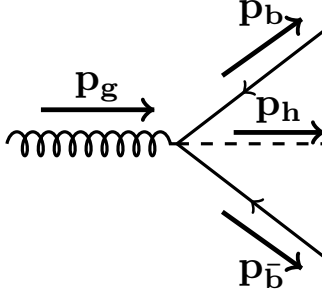


Figure 2. This diagram shows  $s$ -channel gluon production of  $b\bar{b}h$ . Note that, in contrast to SM processes where the Higgs must be radiated from a fermion, here the amplitude is proportional to the gluon momentum, which scales directly with the momentum of the Higgs:  $\mathbf{p}_g = \mathbf{p}_b + \mathbf{p}_{\bar{b}} + \mathbf{p}_h$ . The process  $pp \rightarrow b\bar{b}$  proceeds through the same diagram, with the Higgs set to its vacuum expectation value; there  $\mathbf{p}_g = \mathbf{p}_b + \mathbf{p}_{\bar{b}}$ .

mass energies they correspond to are still small compared to  $\Lambda$ .

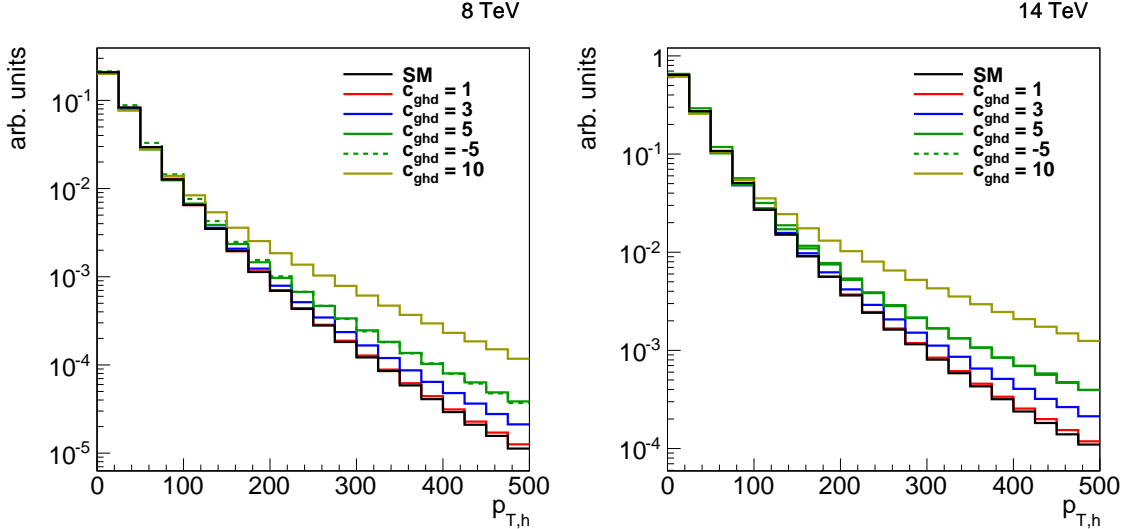


Figure 3. The parton level transverse momentum of the Higgs boson in  $b\bar{b}h$  final states (at leading order) is shown for five different values of the coupling  $c_{ghd}$ . The black, red, blue, dashed green, green, and yellow lines, listed from bottom to top, show the Higgs  $p_T$  for  $c_{ghd} = 0, 1, 3, +5, -5$ , and  $10$ , respectively. These plots are made assuming an equal number of events for each distinct value of  $c_{ghd}$ , hence the kinematic differences arise independent of new physics alterations to the total cross-section for  $pp \rightarrow b\bar{b}h$ . The left plot shows the distributions for 8 TeV, and the right plot contains the 14 TeV distributions. Both sets of curves were generated with CTEQ6L parton distribution functions, default scale choices, and all parton-level cuts set to default MadGraph5 aMC@NLO values.

Another way to present the kinematic effect of  $\mathcal{O}_{ghd}$  is via cumulative  $p_T$  distributions, i.e. the number of Higgses with  $p_T > p_{T,cut}$ , divided by the corresponding number in the SM, as a function of  $p_{T,cut}$ . The cumulative distributions are shown below in Fig. 4 for the same set of  $c_{ghd}$  as in Fig. 3. The distributions show the same trend as Fig. 3, though the fact that we have integrated over several  $p_T$  bins makes the differences between smaller  $c_{ghd}$  more evident. As one example, for a  $p_{T,h}$  cut of 200 GeV, we expect approximately twice as many events in a  $c_{ghd} = 5$ , “SM +  $\mathcal{O}_{ghd}$ ”

scenario than in the SM.

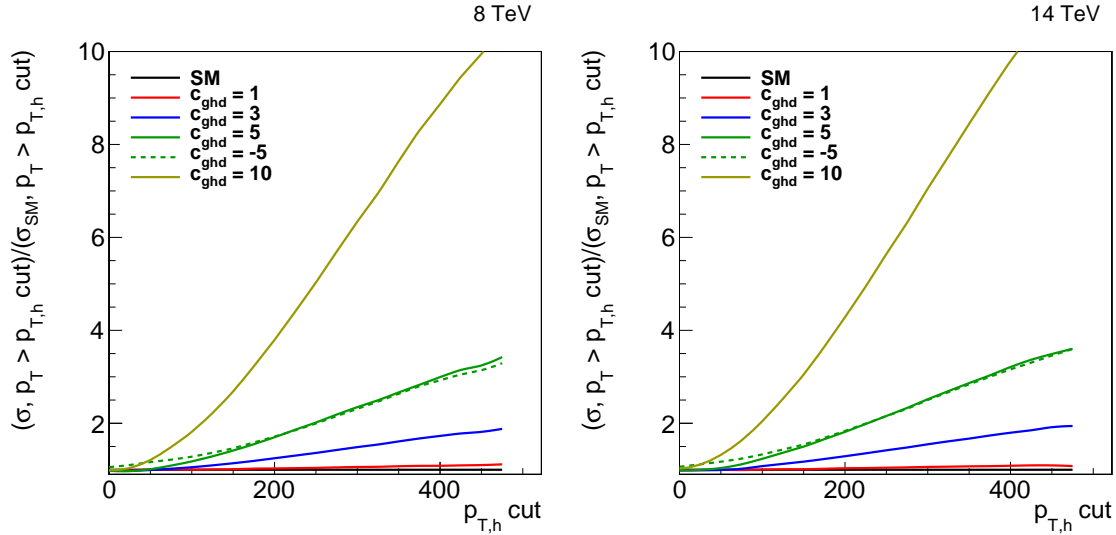


Figure 4. The rate of parton-level, leading order  $pp \rightarrow b\bar{b}h$  events with Higgs  $p_T$  above a set cut value  $p_{T,cut}$  as a function of  $p_{T,cut}$ . The number is normalized to the SM rate after applying the the same cut criteria. A number of different  $c_{ghd}$  values are shown, using the same coloring scheme as Fig. 3 (from bottom to top, the curves are for  $c_{ghd} = 0, 1, 3, +5, -5,$  and  $10,$  respectively).

## B. Quark chirality and the chromomagnetic dipole

In addition to dependence on the gluon momentum, another important structural difference between  $\mathcal{O}_{ghd}$  and the SM is the chirality of the  $b$  quarks. All of the interactions generated from  $\mathcal{O}_{ghd}$  involve a pair of bottom quarks with opposite chirality ( $b_L^\dagger b_R$  or  $b_R^\dagger b_L$ ), while the SM quark chirality depends on the interaction; for QCD gauge interactions, the participating quarks have the same chirality, while for Higgs interactions the quarks have opposite chirality<sup>2</sup>. To see how the  $b$ -quark chirality difference changes things, let us compare SM and SM +  $\mathcal{O}_{ghd}$  contributions to  $pp \rightarrow b\bar{b}$ . Starting with a  $gg$  initial state (though the same argument will work with  $q\bar{q}$ ), we form  $gg \rightarrow b\bar{b}$  by sewing in either one triple-gluon interaction and one  $b\bar{b}g$  interaction or two  $b\bar{b}g$  interactions. In either case, the two outgoing  $b$  quarks have the same chirality if we use only SM QCD interactions. Swapping out one of the SM  $b\bar{b}g$  vertices for the  $\mathcal{O}_{ghd} b\bar{b}g$  vertex, the outgoing bottom quarks now have opposite chirality. In order for these two  $gg \rightarrow b\bar{b}$  contributions to interfere, the chirality on one of the bottom quark lines needs to flip via a mass insertion. Thus, SM- $\mathcal{O}_{ghd}$  interference at leading order (i.e. linear in  $c_{ghd}$ ) in  $pp \rightarrow b\bar{b}$  is suppressed by a factor of  $m_b$ .

The same line of logic, though slightly more complicated, holds for  $pp \rightarrow b\bar{b}h$ . In the SM, the  $b\bar{b}h$  final state arises by dressing the  $pp \rightarrow b\bar{b}$  diagrams discussed above with a Higgs emission on one of the  $b$  quark lines. The outgoing quarks therefore always have opposite chirality. At leading order in  $c_{ghd}$ , the bottom quark chirality depends on whether the diagram involves the  $b\bar{b}g$  vertex contained in  $\mathcal{O}_{ghd}$  or the  $b\bar{b}gh$  vertex. If the diagram contains a  $\mathcal{O}_{ghd} b\bar{b}g$  vertex, the outgoing  $b$  have the same chirality because there are two chirality flips – one in the  $\mathcal{O}_{ghd}$  vertex and one in

<sup>2</sup> We are ignoring electroweak interactions here as they are subdominant, and we only mention the Higgs interaction because we are interested in final states containing Higgses.

the subsequent Higgs emission (via a SM vertex). However, if the diagram contains a  $\mathcal{O}_{ghd} \bar{b}\bar{g}h$  vertex the  $b$  and Higgs are emitted from the same vertex, thus there is only one chirality flip and the outgoing quarks have opposite chirality.

The chirality structure of  $pp \rightarrow \bar{b}b$  and  $pp \rightarrow \bar{b}bh$  in the SM and  $\mathcal{O}_{ghd}$  is summarized below in Table I. Any time the SM and  $\mathcal{O}_{ghd}$  contributions have different chirality, interference between the two is suppressed by  $m_b$ .

Model	Process	Quark Chirality
SM	$pp \rightarrow \bar{b}b$	S
SM	$pp \rightarrow \bar{b}bh$	O
$\mathcal{O}_{ghd}(bbg)$	$pp \rightarrow \bar{b}b$	O
$\mathcal{O}_{ghd}(\bar{b}bg)$	$pp \rightarrow \bar{b}bh$	S
$\mathcal{O}_{ghd}(\bar{b}bgh)$	$pp \rightarrow \bar{b}bh$	O

Table I. Chirality of the outgoing bottom quarks in  $pp \rightarrow \bar{b}b$  and  $pp \rightarrow \bar{b}bh$  events within the SM and with leading order  $\mathcal{O}_{ghd}$  effects: S stands for same chirality, and O for opposite. The  $\mathcal{O}_{ghd}$  vertex is indicated in parenthesis in the first column.

### C. Other operators and general EFT remarks

Having identified the structural aspects of  $\mathcal{O}_{ghd}$  that lead to non-SM kinematics, we can inspect other dimension-6 operators for similar features. The dimension-6 operators that include  $b$  quarks and Higgses are

$$\begin{aligned}
\mathcal{O}_{bHq} &= (Q_3^\dagger \bar{\sigma}^\mu Q_3)(H^\dagger \overleftrightarrow{D}_\mu H), & \mathcal{O}_{c'Hd} &= (Q_3^\dagger \tau_i \bar{\sigma}^\mu Q_3)(H^\dagger \tau^i \overleftrightarrow{D}_\mu H), \\
\mathcal{O}_{cHd} &= (\bar{b}^{c\dagger} \bar{\sigma}^\mu b^c)(H^\dagger \overleftrightarrow{D}_\mu H), & \mathcal{O}_{y_d} &= H^\dagger H Q_3^\dagger H b^{c\dagger} + h.c.,
\end{aligned}
\tag{7}$$

where  $\tau^i$  are the  $SU(2)_w$  generators. The first three operators always contain an electroweak gauge boson; they correct the  $\bar{b}bZ$ ,  $\bar{b}tW$ , etc. vertices and lead to 4-particle  $\bar{b}bW/Zh$  interactions. At  $\mathcal{O}(\alpha_s)$ , these processes do not affect  $pp \rightarrow \bar{b}b$ ,  $pp \rightarrow \bar{b}bh$ , or  $pp \rightarrow h$ . In order to accommodate electroweak precision constraints the couplings multiplying  $\mathcal{O}_{bHq}$ ,  $\mathcal{O}_{c'Hd}$ , and  $\mathcal{O}_{cHd}$  must be so small that they are unlikely to appreciably alter LHC measurements. The fourth operator,  $\mathcal{O}_{y_d}$ , modifies the relation between the  $b$  mass and the Yukawa coupling, but it has the same Yukawa structure as the SM. Thus the effects of  $\mathcal{O}_{y_d}$  can be subsumed into a rescaling of the SM rate.

There are also dimension-six operators that contain only a subset of the fields we are interested in –  $\bar{b}b$ , Higgs, or gluon – but which can affect both the rate and kinematics of  $\bar{b}bh$  events. One such operator is

$$\mathcal{O}_{GH} = (H^\dagger H)(G_{\mu\nu}^a G_a^{\mu\nu}),
\tag{8}$$

which can feed into  $pp \rightarrow \bar{b}bh$  as shown below in Fig. 5, carrying non-SM momentum dependence.

However, as  $\mathcal{O}_{GH}$  generates a tree-level contribution to  $pp \rightarrow h$ , its coefficient is highly constrained by LHC Higgs data. It is possible to avoid these constraints by including other operators in addition to  $\mathcal{O}_{GH}$  and tuning the strength of the multiple interactions against each other such that  $pp \rightarrow h$  is within the experimental limits. This sort of tuning is necessary when looking for non-SM kinematic features in  $pp \rightarrow t\bar{t}h$  events [21, 37]. Taken individually, the couplings of  $\mathcal{O}_{GH}$  and the top quark chromomagnetic dipole are constrained to be small. However if both operators are turned on simultaneously they can be arranged to cancel, admitting larger couplings – and



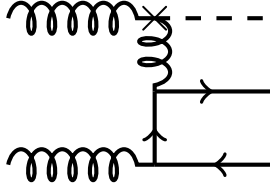


Figure 5. This diagram shows one contribution of the Higgs-gluon kinetic coupling term,  $\mathcal{O}_{GH}$ , to  $b\bar{b}h$  processes at the LHC.

thereby larger effects in Higgs kinematics – without running afoul of bounds. As we will see shortly, the constraints on  $\mathcal{O}_{ghd}$  from inclusive  $pp \rightarrow h$  production are small, hence we are less restrained by phenomenological restrictions, and can omit  $\mathcal{O}_{GH}$  when exploring non-SM Higgs kinematics in  $b\bar{b}h$  events.

In this study we will focus solely on the chromomagnetic  $b$ -quark operator  $\mathcal{O}_{ghd}$ . This means that our analysis neglects any higher order (dimension 6 and above) operators that may only include gluons, bottoms quarks or the Higgs. A rationale for this approach is as follows: without a UV completion, evaluating the effect of a truncated set of cutoff-suppressed operators is a delicate and potentially ambiguous task. The chromomagnetic dipole is the lowest dimension operator that gives a non-SM kinematic morphology to  $b\bar{b}h$  events. So while other  $\text{dim} \geq 6$  operators may change the rate of  $b\bar{b}h$ , a search for  $\mathcal{O}_{ghd}$  will be sensitive to both these changes and shifts in final state particle kinematics.

One has to pay special attention to the choice of the cutoff suppressing the  $\mathcal{O}_{ghd}$  operator. For a given effective cutoff, absorbing all powers of couplings into the scale  $\Lambda_{\text{eff}}$  means that effects from neglected  $d > 6$  terms are naively suppressed relative to lower order terms by powers of  $\sqrt{\hat{s}}/\Lambda_{\text{eff}}$ . There could be some subtleties regarding unnaturally small couplings or operators generated by loop diagrams that are impossible to address in an effective field theory without the benefit of a UV completion. Our dilemma is similar to that faced by mono-jet dark matter collider searches (e.g. Ref. [53–56]), where the cuts imposed on the initial state jet are often close to the scale suppressing the SM-DM interactions.

To illustrate, note that as we increase the coefficient  $c_{ghd}$  for fixed  $\Lambda$ , the effective cutoff  $\Lambda_{\text{eff}}$  decreases. For smaller values of  $c_{ghd}$ ,  $\sqrt{\hat{s}}/\Lambda_{\text{eff}}$  will always be much less than one for LHC energies, but for larger values of  $c_{ghd}$  one can start getting into a situation where the LHC has probed  $\sqrt{\hat{s}} > \Lambda_{\text{eff}}$ , but not necessarily in the process we are bounding. The highest scale probed so far in a process affected by  $\mathcal{O}_{ghd}$  ( $pp \rightarrow b\bar{b}$ ) is  $\sim 3$  TeV. When bounding  $\mathcal{O}_{ghd}$ , we will encounter processes that can only be seen in current or future LHC data when  $\Lambda_{\text{eff}} < 6$  TeV. We quote these bounds with the caution that they are more a statement of what it takes to deviate from the SM and what sort of UV physics is allowed rather than an actual coupling value. For example, quoting a bound  $\Lambda_{\text{eff}} \sim 1$  TeV requires that whatever UV completion kicks in at 1 TeV not disrupt high-mass  $pp \rightarrow b\bar{b}$  studies. In order to remain agnostic towards the UV completion of the theory, we will consider cutoffs as small as  $\Lambda_{\text{eff}} \gtrsim 1$  TeV, although as just explained, cutoffs smaller than  $\sim 3$  TeV should be considered heuristic, because e.g. any resonant  $s$ -channel production of  $b\bar{b}$  at this energy would likely have been seen in  $b\bar{b}$  dijet studies. For a detailed discussion of the delicate issues surrounding the task of bounding effective field theories with data from colliders, see Ref. [57].

### III. CONSTRAINTS ON THE BOTTOM QUARK CHROMOMAGNETIC DIPOLE

Because devoted SM Higgs plus jets studies including  $b$ -tags have not yet been conducted at the LHC, the chromomagnetic dipole operator  $\mathcal{O}_{ghd}$  remains unconstrained from direct  $pp \rightarrow b\bar{b}h$  measurements. However, a number of other processes affected by a  $b$ -quark chromomagnetic dipole can put an upper bound on  $c_{ghd}$ .

Before determining non- $b\bar{b}h$  LHC particle production constraints on  $\mathcal{O}_{ghd}$ , we comment on how  $\mathcal{O}_{ghd}$  affects static Higgs properties. Specifically,  $\mathcal{O}_{ghd}$  contributes to the three-body Higgs decay mode  $h \rightarrow b\bar{b}g$ . In principle this changes the Higgs width, which affects all Higgs branching ratios. In practice we find this partial width is small, less than 1/1000 of the total Higgs width for  $O(1)$  values of  $c_{ghd}$ , so that the total Higgs width is essentially independent of  $c_{ghd}$  for the range of values considered in this study. Note that Higgs width and branching ratio constraints are more severe on other possible higher-dimension Higgs-bottom quark interactions which contribute directly to  $h \rightarrow b\bar{b}$ , such as  $\mathcal{O}_{yb} = (H^\dagger H)(Q^\dagger H) y_b b^c$ .

#### A. $b$ -jet production; $pp(\bar{p}) \rightarrow b\bar{b}$

In Ref. [37], it was shown that measurements of the inclusive  $pp \rightarrow t\bar{t}$  cross-section set strong constraints on the size of the top quark chromomagnetic dipole, the up-type quark cousin of the operator in Eq. (5):

$$\mathcal{O}_{ght} \sim \frac{c_{ght}}{\Lambda_0^2} (Q_3 H) y_t \sigma_{\mu\nu} t^A t^c G_A^{\mu\nu}. \quad (9)$$

Using the same convention as in Eq. (6), we can combine the Yukawa coupling and original cutoff  $\Lambda_0$  into a new cutoff,  $y_t/\Lambda_0^2 = 1/\Lambda^2$ . However, as the top Yukawa is nearly 1,  $\Lambda$  and  $\Lambda_0$  are approximately equal.

For a cutoff scale  $\Lambda_0 = 1$  TeV, the LHC  $pp \rightarrow t\bar{t}$  measurements [58–61] restrict  $c_{ght}$  to  $-1 \lesssim c_{ght} \lesssim 0.5$ . Based on this observation, one might expect measurements of  $pp \rightarrow b\bar{b}$  to have a similar impact on the size of  $c_{ghd}$ , the coefficient of  $\mathcal{O}_{ghd}$ . However, this expectation is not correct for a couple of reasons. First, the SM cross section  $pp \rightarrow b\bar{b}$  is orders of magnitude larger than  $pp \rightarrow t\bar{t}$  and is dominated by low energy scattering at  $\hat{s} \sim 4m_b^2$ . The effect of  $\mathcal{O}_{ghd}$  is suppressed at these low energies, making the inclusive  $pp \rightarrow b\bar{b}$  cross section a useless observable for bounding  $c_{ghd}$ . To have any chance at sensitivity to  $\mathcal{O}_{ghd}$ , we must focus on the most energetic  $pp \rightarrow b\bar{b}$  collisions. To date, the best measurement of  $b\bar{b}$  production at large center-of-mass energies has been set by a CMS study excluding heavy  $b\bar{b}$  resonances with invariant mass ranging from  $\sim 1 - 5$  TeV [62].

A second reason the lesson from  $pp \rightarrow t\bar{t}$  does not carry over to  $pp \rightarrow b\bar{b}$  is interference. As mention in Sec. II B, the chromomagnetic moment operators lead to gluon-quark-quark interactions with a different chirality structure than the usual SM vertex, thus interference between new physics and the SM must be proportional to the quark mass. As a result, interference in  $pp \rightarrow b\bar{b}$  is highly suppressed, while in  $pp \rightarrow t\bar{t}$  it is not.

Finally, when comparing  $\mathcal{O}_{ghd}$  and  $\mathcal{O}_{ght}$ , we must remember our cutoff convention. While the convention choice does not change the results, when comparing different operators, we have to make sure we use the same rules. As  $y_t \sim 1$  there is no difference between the initial cutoff  $\Lambda_0$  and the rescaled cutoff  $\Lambda$ , while the small value of  $y_b$  leads to  $\Lambda \sim 6\Lambda_0$ . Stated another way, a coefficient  $c_{ght} = 1$  leads to the same overall operator strength as  $c_{ghd} = 40$ .

To determine the sensitivity of high-mass  $pp \rightarrow b\bar{b}$  searches to the bottom quark chromomagnetic operator, we mimicked the analysis of Ref. [62]. Specifically, we generated  $pp \rightarrow b\bar{b}$  events at

$\sqrt{s} = 8$  TeV using the “SM +  $\mathcal{O}_{ghd}$ ” Madgraph model introduced in Sec. II A for several different  $c_{ghd}$  values. These parton level events were subjected to the following cuts: 2 or more jets (anti- $k_T$ , jet radius 0.5, and  $p_T > 30$  GeV), with the leading two jets satisfying  $|\eta_j| < 2.5$ ,  $\Delta\eta_{jj} < 1.3$  and  $m_{jj} > 1$  TeV. We plot the relative SM and “SM +  $\mathcal{O}_{ghd}$ ” rate per dijet invariant mass bin in Fig. 6. We do not simulate parton showering and detector acceptance, since these will affect SM and new physics  $b\bar{b}$  equally.

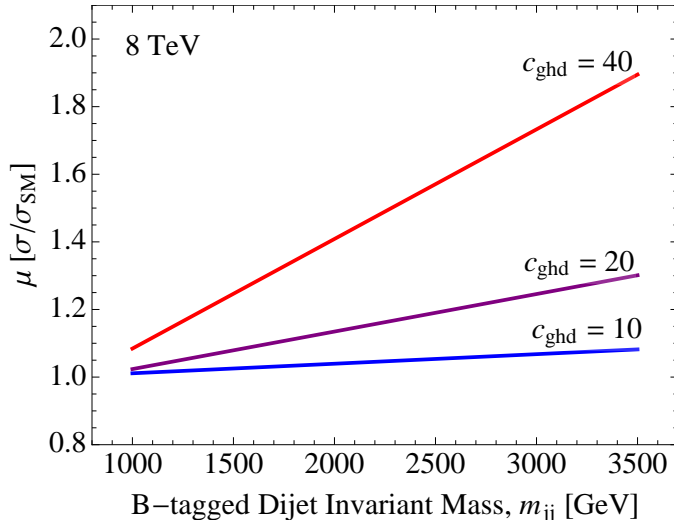


Figure 6. This plot shows the ratio of new physics to Standard Model  $pp \rightarrow b\bar{b}$  cross-sections ( $\mu^{\text{parton}} = \frac{\sigma}{\sigma_{SM}}$ ) plotted against the  $b$  quarks’ dijet invariant mass, for chromomagnetic dipole couplings ( $c_{ghd}$ ) as indicated, and for  $\sqrt{s} = 8$  TeV proton collisions. Additional cuts applied included requiring 2 or more jets with  $p_T > 30$  GeV), with  $|\eta_j| < 2.5$ , and  $m_{jj} > 1$  TeV. Measurements of the area normalized cross-section vs.  $b$ -tagged dijet invariant mass [62] indicate that  $c_{ghd} = 40$  is ruled out, while  $c_{ghd} = 20, 10$  are allowed at  $\sim 95\%$  confidence.

Because the LHC measurement [62] normalizes dijet mass distributions to the shape of SM Monte Carlo distributions and is not an absolute cross-section measurement, it is insensitive to overall shifts in  $b\bar{b}$  rates. For a very large value of  $c_{ghd} = 40$  (meaning a cutoff  $\Lambda = 1$  TeV), we find that current  $pp \rightarrow b\bar{b}$  are barely sensitive to  $\mathcal{O}_{ghd}$ , and this affect would require careful comparison of event rates in low and high invariant mass bins. Specifically, for  $c_{ghd} = 40$ , we find the rate difference between the SM and the SM augmented by  $\mathcal{O}_{ghd}$  in  $1 \text{ TeV} \leq m_{bb} \leq 5 \text{ TeV}$  events is nearly double, which is excludable using the dijet invariant mass event distributions in [62]. The dijet invariant mass event bins of [62] have  $1\sigma$  error bars of  $\sim 20\%$ , so a bin-to-bin shift in expected event rate must be roughly double for a  $5\sigma$  exclusion. This qualitative comparison was carried out only at the parton level. We do not expect showering, hadronization, and detector effects to significantly change the story, especially as the event rate is fitted to the data and no detailed event counts or error bars are given in [62].

A final complication in these  $pp \rightarrow b\bar{b}$  limits on  $\mathcal{O}_{ghd}$  is how we model the proton, i.e. the parton distribution functions. The bottom quark is light enough that it can compose a non-negligible fraction of sufficiently high-energy protons. Admitting initial state  $b/\bar{b}$  quarks leads to new contributions to  $pp \rightarrow b\bar{b}$ , thereby introducing new ways  $\mathcal{O}_{ghd}$  can enter. However, we find that including  $b$  quarks as initial state partons enhanced  $pp \rightarrow b\bar{b}$  rates for the SM and  $c_{ghd} = 40$  equally, in each case increasing the cross-section by  $\sim 3\%$  in each  $b\bar{b}$  invariant mass bin (CTEQ6L parton distribution functions). Since the normalization shift is the same with and without  $\mathcal{O}_{ghd}$ ,

the addition of  $b$  quark partonic states does not alter the constraints on  $c_{ghd}$  presented in Figure 6.

We conclude that current studies of high invariant mass  $b\bar{b}$  production are not sensitive to the  $b$  quark chromomagnetic dipole for couplings less than  $c_{ghd} = 40$ . As we have discussed, this is partly because the interference of the  $b$  quark chromomagnetic operator's  $pp \rightarrow b\bar{b}$  production and SM  $b\bar{b}$  production requires a chirality flip for one of the  $b$  quarks, and a corresponding suppression from the bottom quark mass, as illustrated in Fig. 1.

### B. Inclusive Higgs production: $pp \rightarrow h$

Having shown that  $pp \rightarrow b\bar{b}$  events do not place any strong constraint on the chromomagnetic bottom quark operator, we now explore constraints from SM Higgs production at 7 and 8 TeV. Because  $\mathcal{O}_{ghd}$  is generated at the scale  $\Lambda$ , if we evolve down to the scale relevant to Higgs production via the renormalization group, the loop-level effects of  $\mathcal{O}_{ghd}$  can be subsumed into an altered coefficient for the effective  $h G_A^{\mu\nu} G_A^{\mu\nu}$  operator:

$$\mathcal{L} \supset c_{hgg}^{SM} h G_A^{\mu\nu} G_A^{\mu\nu} \rightarrow \left( c_{hgg}^{SM} + \frac{c_{ghd} m_b}{16\pi^2 \Lambda^2} \log\left(\frac{\Lambda}{m_b}\right) \right) h G_A^{\mu\nu} G_A^{\mu\nu}, \quad (10)$$

where  $c_{gg}^{SM}$  is the usual SM contribution coming from top quark loops.

One might expect that the above alteration of Higgs boson production would be the most constraining result of a bottom quark chromomagnetic dipole, especially since prior studies of the top quark chromomagnetic dipole found this to be the case for the top quark [21, 37].

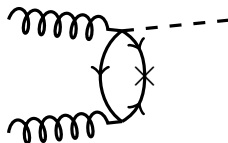


Figure 7. This diagram shows one contribution of the bottom quark chiral-dipole operator (4) to Higgs boson production at the LHC. Note that the chirality flip in the quark loop will introduce a suppression proportional to the bottom Yukawa  $y_b$  for the case of a  $b$  quark chromomagnetic dipole contributing to Higgs boson production.

However, the  $b$ -quark lines emanating from  $\mathcal{O}_{ghd}$  have opposite chirality. Therefore, following the same logic as in Sec. IIB, in order to close the  $b$ -quark lines from  $\mathcal{O}_{ghd}$  into a loop contribution to  $gg \rightarrow h$ , a mass insertion on one of the internal quark lines is required. The chirality structure for a sample diagram is shown explicitly in Fig. 7. This mass insertion causes the extra factor of  $m_b$  in the second term in Eq. (10) which, since  $m_b$  is much less than the other scales ( $\Lambda$  or  $v$ ), strongly suppresses the  $\mathcal{O}_{ghd}$  contribution. An analogous chirality flip is required to generate a  $gg \rightarrow h$  contribution from the top-quark chromomagnetic operator, as done in Ref. [21, 37]. However, in that case the large mass of the top quark makes the mass-insertion suppression price much less severe.

Plugging representative numbers into Eq. (10), we see that for a cutoff of  $\Lambda = 6$  TeV, the change<sup>3</sup> in  $c_{hgg}$  is very small:  $\delta c_{hgg} \sim 10^{-4}$  for  $c_{ghd} = 1$ . For larger  $c_{ghd}$ ,  $\delta c_{hgg}$  increases, but only

<sup>3</sup> We use  $c_{hgg} \simeq \frac{\alpha_s(m_Z)}{3\pi v} \left(1 + \frac{7}{30}x + \frac{2}{21}x^2\right)$  where  $x \equiv \frac{m_b^2}{4m_t^2}$ .

linearly with  $c_{ghd}$ . In order to have a noticeable effect on inclusive Higgs production, the coupling would need to be  $O(100)$ , an unreasonably large value from the EFT perspective. We conclude that inclusive Higgs production is not a sensitive probe of the bottom quark chromomagnetic dipole operator. This should be contrasted with the top-quark chromomagnetic dipole: there corrections to  $c_{hgg}$  from the dipole contribution are so large that  $c_{ght}$  is constrained – for  $\Lambda = \text{TeV}$  and assuming no other higher-dimensional operators – to  $\lesssim O(1)$ .

### C. Higgs plus dijets: $pp \rightarrow h + jj$

We now address a final state at the LHC which has the potential to constrain  $\mathcal{O}_{ghd}$ ,  $pp \rightarrow h + jj$ . While there is no dedicated  $\bar{b}b + h$  search,  $\bar{b}b h$  events will show up in any Higgs plus jets search provided bottom quarks are not explicitly vetoed. The  $pp \rightarrow \bar{b}b h$  final state looks promising since, as we saw in Sec. II A and II B, the SM- $\mathcal{O}_{ghd}$  interference is not suppressed by  $m_b$ , and it is possible to enhance the  $\mathcal{O}_{ghd}$  effects by looking at regions of phase space where  $\sqrt{\hat{s}}$  is large.

The Higgs plus jets channel with the tightest constraint on new physics contributions is the diphoton decay mode,  $h(\gamma\gamma) + jj$ ; specifically, the rate in this channel in any extension of the SM relative to the SM – the signal strength  $\mu^{\text{collider}}$  – is restricted to  $0.8 \pm 0.7$  by ATLAS [63]<sup>4</sup>, and  $\mu_{hjj}^{\text{collider}} = 1.11^{+0.32}_{-0.30}$  by CMS [64]. Since  $\mathcal{O}_{ghd}$  has a different structure than the SM, we do not expect SM and “SM +  $\mathcal{O}_{ghd}$ ” events to have the same cut acceptance. Therefore, in order to see how the signal strength limits translate into bounds on  $c_{ghd}$ , we have to rely on Monte Carlo simulation. Specifically, we simulate the CMS analysis of  $pp \rightarrow h + jj \rightarrow \gamma\gamma + jj$  final states [64] for a number of values of  $c_{ghd}$  and a cutoff of  $\Lambda = 6 \text{ TeV}$ , then compare with the SM prediction. The signal events are generated at parton level using the Madgraph “SM +  $\mathcal{O}_{ghd}$ ” model, passed through Pythia 8.1 [65] for showering and hadronization, then routed through Delphes [66] to incorporate detector effects<sup>5</sup>. We then apply the following cuts, taken from the CMS analysis [64]:

- (1) The highest  $p_T$  photon must be larger than half the invariant mass of the photon pair,  $p_{T,\gamma_1} > m_{\gamma\gamma}/2$ , and the second highest  $p_T$  photon must satisfy  $p_{T,\gamma_2} > 25 \text{ GeV}$ .
- (2) The diphoton invariant mass,  $m_{\gamma\gamma}$ , must be between 120 GeV and 130 GeV.
- (3) The two leading jets must have  $|\eta| < 4.7$ .
- (4) The difference in azimuthal angle between the dijet and diphoton systems ( $\Delta\phi_{jj-\gamma\gamma}$ ) must be greater than 2.6.
- (5) The Zeppenfeld variable  $Z = \eta[\gamma_1 + \gamma_2] - (\eta[j_1] + \eta[j_2])/2$  must be less than 2.5.
- (6) The difference in pseudorapidity between the jets ( $\Delta\eta_{jj}$ ) must be greater than 3.
- (7) For the dijet tight (dijet loose) cut the invariant mass of the jets must be  $> 500 \text{ GeV}$  ( $> 250 \text{ GeV}$ ) and both jets must have  $p_T > 30 \text{ GeV}$  (the second highest  $p_T$  jet must have  $p_T > 20 \text{ GeV}$ ).

<sup>4</sup> ATLAS categorizes diphoton Higgs events by their production mechanism rather than the final state. The number quoted is the vector boson fusion (VBF) category. While VBF events should comprise a large fraction of  $h + jj$  events, the two rates are not equal. For this reason, we use the CMS numbers and procedure throughout this section.

<sup>5</sup> We use the default Delphes CMS detector card in all analyses.

	Measured ([64])	$c_{ghd} =$	-40	-20	0	20	40
$\mu_{hjj}$	$1.11^{+0.32}_{-0.30}$		1.19	1.03	1	1.04	1.24

Table II. This table shows the expected rate parameter  $\mu_{hjj}^{\text{collider}}$  in a CMS study of  $pp \rightarrow h + jj \rightarrow \gamma\gamma + jj$  for indicated values of a chromomagnetic bottom quark coupling  $c_{ghd}$  with a cutoff of  $\Lambda = 6$  TeV. The signal strength  $\mu_{hjj}^{\text{collider}}$  is calculated after collider-level cuts have been applied. The signal events were generated via MadGraph 5, Pythia, and Delphes at  $\sqrt{s} = 8$  TeV as described in the text. Cuts were implemented to match those of [64], and the rate from the CMS study  $\mu_{hjj}^{\text{collider}} = 1.11^{+0.32}_{-0.30}$  is displayed for reference.

Post-cuts, we compare the rate relative to the Standard Model expectation (obtained by simulating SM events without the addition of a bottom quark chromomagnetic dipole), and these ratios of rates for several  $c_{ghd}$  are shown in Table II. We find that for a cutoff of  $\Lambda = 6$  TeV, even couplings as large as  $|c_{ghd}| \sim 40$  are not constrained by the most recent Higgs plus jets studies.

Of course, a coupling this large and  $\Lambda = 6$  TeV corresponds to the same effective cutoff as an order one coupling and  $\Lambda = 1$  TeV. Depending on the UV model inducing the chromomagnetic dipole, order one couplings for such a 1 TeV cutoff would be at odds with  $b\bar{b}$  di-jet resonance studies, which do not show any deviation from a Standard Model invariant mass distribution. We discussed the bound on 1-6 TeV di-b-jet invariant mass distributions in Section III A and found  $pp \rightarrow b\bar{b}$  insensitive to  $\mathcal{O}_{gdb}$ , however the bounds derived there were under the assumption that the *only* new physics effect was the chromomagnetic moment. If the cutoff  $\Lambda_{\text{eff}}$  of the EFT is within the energy reach of  $pp \rightarrow b\bar{b}$ , we must include all the physics at  $\Lambda_{\text{eff}}$  – either in the form of on-shell states or dimension  $> 6$  operators – in order to get a meaningful bound. Stated another way, one cannot simply take  $c_{ghd} \sim 40$ ,  $\Lambda = 6$  TeV as an indication of the scale of some new physics without explaining via UV model building why experiments involving  $b, \bar{b}, g$  or Higgs that are sensitive to  $\sqrt{s} > \Lambda_{\text{eff}}$  show no deviation.

Regardless of the UV physics being probed, it is clear from Table II that flavor-blind  $hjj$  studies are insensitive to the  $b$  quark chromomagnetic dipole.

#### IV. PRESS THE $b$ -TAG BUTTON

Having seen that existing flavor blind  $h + jj$  studies place no bound on  $\mathcal{O}_{ghd}$ , we now explore how requiring  $b$ -tags and modifying the cuts can improve the sensitivity. We first build off of the 8 TeV LHC analysis discussed in the previous section [64], then present a more optimized approach for use at a high luminosity run of the 14 TeV LHC. For the relatively low luminosity collected at 8 TeV, the cuts applied will need to be parsimonious to obtain substantial exclusion significance.

##### A. Constraints on $b\bar{b}h$ at the 8 TeV LHC

In addition to cuts (1)-(3) given in Subsection III C, for a  $b\bar{b}h$  study at 8 TeV we also require that

- The event must have one jet that passes the medium selection criteria detailed in [67] (70% b-jet tagging, 1.5% light quark miss-tagging).
- The  $p_T$  of the vector sum of the diphoton momenta must be greater than 150 GeV.

For this study, we modify the default CMS Delphes card to tag 70% of the  $b$ -jets in our simulated events, and miss-tag 1.5% of the light quarks as  $b$ -jets. While we retain cuts (1)-(3) from the CMS

analysis, the remaining four are dropped. These latter cuts, in particular the cut on the Zeppenfeld variable [68], are designed to pick out Higgs events produced via vector boson fusion (VBF). While separating Higgs plus jets events into “gg-initiated” and “VBF” categories is an extremely useful tool for pinning down exactly how the Higgs couples to vector bosons vs. gluons, these cuts do more harm than good for our  $b\bar{b}h$  signal. There are several  $pp \rightarrow b\bar{b}h$  diagrams that have similar topology to VBF-initiated Higgses, however the feature of  $\mathcal{O}_{ghd}$  we really want to exploit is the momentum dependence. We find better results by dropping these VBF-specific cuts in favor of the cut directly on the diphoton (Higgs)  $p_T$ .

As we have modified the analysis, we can no longer use quoted CMS backgrounds. In order to simulate background events arising from non-Higgs  $jj\gamma\gamma$  final states, and to check our collider simulations against the CMS result, we produced a background sample of  $pp \rightarrow jj\gamma\gamma$  and  $pp \rightarrow b\bar{b}\gamma\gamma$  events in Madgraph. We then followed the same procedures as previously outlined for showering and detector simulation of this background<sup>6</sup>.

The results from this modified,  $b$ -tag enhanced analysis are listed in Table III for a sampling of  $c_{ghd}$  values. We quote event counts for  $20 \text{ fb}^{-1}$  of integrated luminosity.

	$jj\gamma\gamma$ bkgd	$b\bar{b}\gamma\gamma$ bkgd	$c_{ghd} =$	-40	-20	0	20	40
8 TeV $b\bar{b}h$ events ( $20 \text{ fb}^{-1}$ )	0.2	0.4		1.9	0.5	0.05	0.5	1.8
8 TeV $\mu_{b\bar{b}h}^{\text{collider}}$	–	–		38	10	1	10	36
8 TeV $\mu_{b\bar{b}h}^{\text{parton}}$	–	–		2.7	1.5	1	1.2	2.1

Table III. This table shows the expected number of events for a  $b$ -tagged study of  $b\bar{b}h$  at 8 TeV for  $20 \text{ fb}^{-1}$  of luminosity and a  $\Lambda = 6 \text{ TeV}$  cutoff. In addition to cuts (1)-(3) given in subsection III C, it was additionally required that the vector sum of the diphoton  $p_T$  be greater than 150 GeV and that one of the two highest  $p_T$  jets pass the medium charged secondary vertex  $b$ -tagging requirements detailed in [67]. Cuts (4)-(7) in subsection III C, which target VBF-produced Higgs bosons, were not applied to these events. The relative rate after collider cuts,  $\mu_{b\bar{b}h}^{\text{collider}}$ , can be compared to the tree-level parton cross-section  $\mu_{b\bar{b}h}^{\text{parton}}$ , to see the efficacy of the  $p_T > 150 \text{ GeV}$  cut on the vector summed photons.

Comparing the results in Table III to those in Table II, we find that adding a single  $b$ -tag and requiring the vector summed photon  $p_T > 150 \text{ GeV}$  increases the expected significance of detection or exclusion of the chromomagnetic dipole operator. For a  $c_{ghd} = 40$  coupling and a  $\Lambda = 6 \text{ TeV}$  cutoff, and assuming a Poisson distribution with 0.65 SM events expected and a  $\pm 0.5$  events systematic error, we find an  $O(2\sigma)$  exclusion could be obtained with the current 8 TeV data. As already discussed, if an excess of events were found indicating  $c_{ghd} = 40$  for  $\Lambda = 6 \text{ TeV}$ , this would indicate new physics at scales around a TeV, meaning the new physics responsible would have to avoid resonant  $b\bar{b}$  production that dijet resonance searches have excluded for  $\Lambda \sim 1 \text{ TeV}$ . In Table III we also give the parton-level relative cross-section rate  $\mu_{b\bar{b}h}^{\text{parton}} \equiv \sigma/\sigma_{NP} |_{\text{Parton Level}}$  for SM vs new physics events. We remind the reader that  $\mu_{b\bar{b}h}^{\text{parton}}$  does not include the affect of kinematic cuts, while  $\mu_{b\bar{b}h}^{\text{collider}}$  does. The efficacy of the collider cuts on photon transverse momentum can be observed by comparing  $\mu_{b\bar{b}h}^{\text{parton}}$  to  $\mu_{b\bar{b}h}^{\text{collider}}$  in Table III.

While a  $b$ -tagged search for non-standard  $b\bar{b}h$  rates and kinematics has not yet been conducted, there is a set of inclusive Higgs measurements with  $b$ -tags worth comment, namely searches for MSSM (or 2HDM) Higgses. These searches are typically in the  $pp(\bar{p}) \rightarrow b\bar{b}\Phi(\bar{b}b)$  [69] or

<sup>6</sup> We checked the MadGraph-generated background sample of  $jj\gamma\gamma$  events by using the same cuts implemented in [64], and found that for these cuts, the expected numbers of background events matched those found by the CMS study to within 20%.

$b\bar{b}\Phi(\tau^+\tau^-)$  [70, 71] channels, where  $\Phi$  can stand for any one of the three neutral Higgses in a 2HDM. These final states are chosen to take advantage of the increased bottom quark and tau lepton Yukawa couplings when  $\tan\beta$  is large. However, the bulk of the sensitivity of these searches comes when the second set of neutral Higgses (mass  $m_A$ ) are light. To understand this, recall that in the decoupling limit ( $m_A \rightarrow \infty$ ) the bottom-quark coupling to the light SM Higgs asymptotes to the SM value. The couplings that are actually enhanced are the couplings of the bottom quarks (taus) to the heavy Higgses, therefore the enhancement in MSSM/2HDM  $pp(\bar{p}) \rightarrow b\bar{b}\Phi(\bar{b}b)$  rates falls off as  $m_A$  grows and the heavy states are less abundantly produced. We see from Table III that a chromomagnetic dipole coupling of  $c_{ghd} = 40$  only doubles the expected rate of  $b\bar{b}h$  events, which corresponds to  $\tan\beta \sim \sqrt{2}$ , a small  $\tan\beta$  outside the sensitivity of MSSM/2HDM studies. Hence, recasting MSSM/2HDM  $pp(\bar{p}) \rightarrow b\bar{b}\Phi(\bar{b}b)$  limits in terms of  $\mathcal{O}_{ghd}$ , does not lead to a strong bound. Another way to understand this lack of sensitivity is that, while these MSSM searches look for  $\Phi \rightarrow bb$ , they don't impose a boost requirement on the  $\Phi$ . With no boost requirement, the cross section is dominated by the low- $p_T$  region, where  $\mathcal{O}_{ghd}$  has little effect.

### B. Constraints on $b\bar{b}h$ at the 14 TeV LHC

Of course, sensitivity to  $\mathcal{O}_{ghd}$  via  $b\bar{b}h$  can be improved upon with a high luminosity run at the 14 TeV LHC. As we have the luxury of higher energy and luminosity, we can cut harder on the Higgs  $p_T$  than at 8 TeV, obtaining a better signal to background ratio at the expense of overall rate. In particular, we studied the sensitivity of the 14 TeV LHC to the chromomagnetic bottom quark operator using the following cuts:

- Exactly two photons and two or more jets, all satisfying the same identification criteria (cuts (1)-(3)) as in subsection III C.
- The two highest  $p_T$  jets must pass the tight charged secondary vertex b-tagging requirements (55% tag, 0.1 % light quark mis-tag) detailed in [67]. Whereas at 8 TeV, it was necessary to use the medium CSV b-tag to keep as many  $b\bar{b}h$  events as possible, at 14 TeV we find that removing the  $jjh$  background yields better significance. Note that for both the medium (light) CSV b-tags, we match the results of [67] by assuming that 20% (10%) of charm quarks will fake bottom quark jets.
- The vector sum of diphoton  $p_T$  must be greater than 200 GeV. This cut tends to exclude non-Higgs produced  $b\bar{b}\gamma\gamma$  backgrounds, and further discriminates between an un-boosted Standard Model sample of  $b\bar{b}h$  events, and events with Higgs bosons boosted by the presence of a chromomagnetic dipole operator. This selection for boosted Higgs events can be seen by comparing the ratio of cross-sections  $\mu^{\text{parton}}$ , given in Table IV to the ratio of selected events,  $\mu^{\text{collider}}$ . For example, looking at  $c_{ghd} = 20$ , we see that the cross-section is around 40% larger than in the SM, but the number of expected events after the cut on vector diphoton  $p_T$  is applied is 15 times larger than the SM expectation.
- As with the previous analysis, all cuts tailored to VBF production (cuts (4)-(7) from subsection III C) are dropped.

Repeating the same signal and background generation and analysis chain as in the previous section and assuming  $3\text{ab}^{-1}$  of integrated luminosity, we find the following event counts (Table IV).



	$jj\gamma\gamma$ bkgd	$b\bar{b}\gamma\gamma$ bkgd	$c_{ghd} =$	-20	-10	-5	0	5	10	20
14 TeV $b\bar{b}h$ events ( $3\text{ ab}^{-1}$ )	0.1	7.5		48	13	4	3	5	14	49
14 TeV $\mu_{b\bar{b}h}^{\text{collider}}$	–	–		16	4.3	1.3	1	1.7	4.7	16
14 TeV $\mu_{b\bar{b}h}^{\text{parton}}$	–	–		1.72	1.22	1.08	1	0.99	1.06	1.41

Table IV. The number of expected events are shown for indicated  $c_{ghd}$  couplings and a  $\Lambda = 6$  TeV cutoff at the 14 TeV LHC after  $3\text{ ab}^{-1}$ , after applying cuts (1)-(3) detailed in subsection III C, in addition to requiring that the diphoton  $p_T$  vector sum exceed 200 GeV and that both of the highest  $p_T$  jets pass the tight charged secondary vertex b-tagging requirement (55% tag, 0.1% mis-tag) detailed in [67]. The relative rate  $\mu_{b\bar{b}h}^{\text{parton}}$  of the new physics vs. SM  $b\bar{b}h$  parton-level cross-sections can be compared to the collider-level event ratio  $\mu_{b\bar{b}h}^{\text{collider}}$  to quantify the affect of the  $p_T > 200$  GeV cut on vector summed diphoton transverse momentum. Thus the selection for new physics events is a result of both cross-section rate and the non-standard kinematics of the chromomagnetic dipole.

From Table IV we see that an  $O(2\sigma)$  exclusion of  $c_{ghd} = 5$  could be achieved after  $3\text{ ab}^{-1}$  luminosity<sup>7</sup>. This corresponds to a shift in the effective cutoff from a TeV up to roughly 6 TeV – implying sensitivity to half the LHC’s energy over its lifetime. Note that the ability to probe down to a  $\Lambda \sim 6$  TeV cutoff hinges on the cut on the vector summed diphoton  $p_T > 200$  GeV – this cut preferentially selects boosted events, which will be abundantly produced if the  $b$  quark has a chromomagnetic dipole. A coarse scan over possible values found that a cut of  $p_T > 200$  GeV produced the highest ratio of new physics ( $c_{ghd} = 5$ ) to SM events without driving both to zero; the separation between signal and background increases with the  $p_T$  cut, but the higher the cut value, the lower the overall rate. In summary, we find that the structure of the  $b$  quark chromomagnetic operator can be thoroughly structinized at  $\sqrt{s} = 14$  TeV and high luminosity.

The numbers in Table IV were derived assuming the only Higgs decay mode viable for Higgs plus dijet searches is the  $\gamma\gamma$  mode. This is a safe, though somewhat conservative assumption. Expanding the search to more decay modes will, in principle, improve the reach, though in practice many other decay modes seem quite challenging to observe:  $h \rightarrow b\bar{b}$  has the largest signal rate but must compete with immense QCD backgrounds;  $h \rightarrow WW^*$  – once combined with the accompanying  $b\bar{b}$  – forms the identical final state to  $t\bar{t}$  production; and  $h \rightarrow \tau^+\tau^-$  events reconstruct the Higgs too inefficiently once one takes into account the difficulty in identifying taus. It is possible that multivariate techniques could find enough kinematic differences between these ‘alternate’ signals, i.e.  $pp \rightarrow h(b\bar{b}) + b\bar{b}$ , and the SM background, but dedicated studies beyond the scope of this paper are required.

## V. CONCLUSIONS

Since it is the heaviest quark that hadronizes, and is the easiest to identify at the LHC, the bottom quark opens a unique door onto the vista of new Higgs dynamics. Sensitivity to the chromomagnetic dipole, which has a distinct momentum structure resulting in a non-standard fraction of boosted Higgs bosons, is paramount in the ongoing quest for new physics. In this work we have pinpointed the effects of this single dimension-6 effective operator. A generic UV theory will likely produce several other dimension-6 operators after heavy degrees of freedom are integrated out. Considering the effects of other operators would change the exact numbers of new physics events quoted here, but the efficacy of a search centered on the unique kinematic structure

<sup>7</sup> Here we simply calculate significance as the signal divided by the square root of the expected SM background.

induced by the chromomagnetic dipole would remain unchanged. To wit, searches for these other operators have a scope restricted to the overall rate of  $b\bar{b}h$  production. A focused search for the chromomagnetic dipole boosting Higgs  $p_T$  allows us to probe to higher energy scales: in the case of this study, we find the chromomagnetic dipole could be probed up to effective energy scales of roughly 6 TeV over the course of a high luminosity LHC run.

In this paper, we first cataloged what bounds can be put on the  $b$  quark chromomagnetic dipole from processes  $h \rightarrow b\bar{b}$ ,  $pp \rightarrow h$ ,  $pp \rightarrow b\bar{b}$ , and  $pp \rightarrow hq\bar{q}$ . There are no bounds on the chromomagnetic operator coming from inclusive decays of the Higgs to  $b\bar{b}g$  (less than a thousandth the total width), or loop production of the Higgs; the amplitude for this latter process is suppressed by a factor of the bottom Yukawa stemming from a chirality flip. We have found that  $pp \rightarrow b\bar{b}$  constrains the  $b$  chromomagnetic dipole Wilson coefficient  $c_{ghd} < 40$  for a 6 TeV cutoff. On the other hand, presently available collider studies of Higgs production in association with two jets – which do not employ  $b$ -tagging – do not constrain the  $b$  quark chromomagnetic dipole.

Casting an eye towards future discovery prospects for  $b\bar{b}h$ , we have found that the sensitivity of Higgs plus dijet searches to the  $b$  quark chromo-dipole operator at 8 TeV with  $19.6 \text{ fb}^{-1}$  and particularly at 14 TeV with  $3 \text{ ab}^{-1}$  will be greatly increased with the addition of  $b$ -tagging in addition to cuts on transverse momentum in  $jj\gamma\gamma$  final states. Both 8 and 14 TeV LHC studies of the  $jjh$  channel should include  $b$ -tags to possibly catch the first glimmer of new physics in dijet plus diphoton ( $m_{\gamma\gamma} \sim 125 \text{ GeV}$ ) events.

The effect of the bottom quark chromomagnetic dipole is one example where an upgrade of the LHC to high luminosity will be very beneficial. We have demonstrated that in order to exclude an order one coupling chromomagnetic operator we will need  $3 \text{ ab}^{-1}$  of luminosity, which clearly shows that more statistics will play an essential role in understanding Higgs precision physics. Indeed, it should not be surprising that in order to exclude  $\sim 6 \text{ TeV}$  new physics coupled to the Higgs and bottom quarks at a 14 TeV machine, a high luminosity is required. The HL-LHC is a natural arena to search for new operators that affect Higgs physics not by changing its properties at its pole mass but by changing the kinematic distributions at high momentum transfer.

**Acknowledgements** We thank Kevin Lannon, Bryan Ostdiek, and Anna Woodard for useful conversations. This work was supported in part by the Notre Dame Center for Research Computing through computing resources. The work of AD was partially supported by the National Science Foundation under Grant No. PHY-1215979, and the work of AM was partially supported by the National Science Foundation under Grant No. PHY14-17118.

- 
- [1] C. Burges and H. J. Schnitzer, *Virtual Effects of Excited Quarks as Probes of a Possible New Hadronic Mass Scale*, *Nucl.Phys.* **B228** (1983) 464.
  - [2] C. N. Leung, S. Love, and S. Rao, *Low-Energy Manifestations of a New Interaction Scale: Operator Analysis*, *Z.Phys.* **C31** (1986) 433.
  - [3] W. Buchmuller and D. Wyler, *Effective Lagrangian Analysis of New Interactions and Flavor Conservation*, *Nucl.Phys.* **B268** (1986) 621–653.
  - [4] A. De Rujula, M. Gavela, P. Hernandez, and E. Masso, *The Selfcouplings of vector bosons: Does LEP-1 obviate LEP-2?*, *Nucl.Phys.* **B384** (1992) 3–58.
  - [5] K. Hagiwara, R. Szalapski, and D. Zeppenfeld, *Anomalous Higgs boson production and decay*, *Phys.Lett.* **B318** (1993) 155–162, [[hep-ph/9308347](#)].
  - [6] M. Gonzalez-Garcia, *Anomalous Higgs couplings*, *Int.J.Mod.Phys.* **A14** (1999) 3121–3156, [[hep-ph/9902321](#)].

- [7] O. J. Eboli, M. Gonzalez-Garcia, S. . Lietti, and S. Novaes, *Probing intermediate mass Higgs interactions at the CERN Large Hadron Collider*, *Phys.Lett.* **B478** (2000) 199–207, [[hep-ph/0001030](#)].
- [8] G. Giudice, C. Grojean, A. Pomarol, and R. Rattazzi, *The Strongly-Interacting Light Higgs*, *JHEP* **0706** (2007) 045, [[hep-ph/0703164](#)].
- [9] B. Grzadkowski, M. Iskrzynski, M. Misiak, and J. Rosiek, *Dimension-Six Terms in the Standard Model Lagrangian*, *JHEP* **1010** (2010) 085, [[arXiv:1008.4884](#)].
- [10] J. Espinosa, C. Grojean, M. Muhlleitner, and M. Trott, *First Glimpses at Higgs’ face*, *JHEP* **1212** (2012) 045, [[arXiv:1207.1717](#)].
- [11] A. Azatov and J. Galloway, *Electroweak Symmetry Breaking and the Higgs Boson: Confronting Theories at Colliders*, *Int.J.Mod.Phys.* **A28** (2013) 1330004, [[arXiv:1212.1380](#)].
- [12] I. Low, J. Lykken, and G. Shaughnessy, *Have We Observed the Higgs (Imposter)?*, *Phys.Rev.* **D86** (2012) 093012, [[arXiv:1207.1093](#)].
- [13] J. Ellis and T. You, *Global Analysis of the Higgs Candidate with Mass  $125$  GeV*, *JHEP* **1209** (2012) 123, [[arXiv:1207.1693](#)].
- [14] A. Alloul, B. Fuks, and V. Sanz, *Phenomenology of the Higgs Effective Lagrangian via FeynRules*, [arXiv:1310.5150](#).
- [15] I. Brivio, T. Corbett, O. Eboli, M. Gavela, J. Gonzalez-Fraile, et al., *Disentangling a dynamical Higgs*, *JHEP* **1403** (2014) 024, [[arXiv:1311.1823](#)].
- [16] C. Englert, A. Freitas, M. Muhlleitner, T. Plehn, M. Rauch, et al., *Precision Measurements of Higgs Couplings: Implications for New Physics Scales*, *J.Phys.* **G41** (2014) 113001, [[arXiv:1403.7191](#)].
- [17] A. Hayreter and G. Valencia, *Constraints on anomalous color dipole operators from Higgs boson production at the LHC*, *Phys.Rev.* **D88** (2013) 034033, [[arXiv:1304.6976](#)].
- [18] D. E. Soper and M. Spannowsky, *Finding physics signals with shower deconstruction*, *Phys.Rev.* **D84** (2011) 074002, [[arXiv:1102.3480](#)].
- [19] L. G. Almeida, O. Erdogan, J. Juknevich, S. J. Lee, G. Perez, et al., *Three-particle templates for a boosted Higgs boson*, *Phys.Rev.* **D85** (2012) 114046, [[arXiv:1112.1957](#)].
- [20] A. Katz, M. Son, and B. Tweedie, *Ditau-Jet Tagging and Boosted Higgses from a Multi-TeV Resonance*, *Phys.Rev.* **D83** (2011) 114033, [[arXiv:1011.4523](#)].
- [21] C. Degrande, J. Gerard, C. Grojean, F. Maltoni, and G. Servant, *Probing Top-Higgs Non-Standard Interactions at the LHC*, *JHEP* **1207** (2012) 036, [[arXiv:1205.1065](#)].
- [22] T. Corbett, O. Eboli, J. Gonzalez-Fraile, and M. Gonzalez-Garcia, *Constraining anomalous Higgs interactions*, *Phys.Rev.* **D86** (2012) 075013, [[arXiv:1207.1344](#)].
- [23] T. Corbett, O. Eboli, J. Gonzalez-Fraile, and M. Gonzalez-Garcia, *Robust Determination of the Higgs Couplings: Power to the Data*, *Phys.Rev.* **D87** (2013) 015022, [[arXiv:1211.4580](#)].
- [24] J. Ellis, D. S. Hwang, V. Sanz, and T. You, *A Fast Track towards the ‘Higgs’ Spin and Parity*, *JHEP* **1211** (2012) 134, [[arXiv:1208.6002](#)].
- [25] G. Isidori, A. V. Manohar, and M. Trott, *Probing the nature of the Higgs-like Boson via  $h \rightarrow V F$  decays*, *Phys.Lett.* **B728** (2014) 131–135, [[arXiv:1305.0663](#)].
- [26] G. Isidori and M. Trott, *Higgs form factors in Associated Production*, *JHEP* **1402** (2014) 082, [[arXiv:1307.4051](#)].
- [27] R. V. Harlander and T. Neumann, *Probing the nature of the Higgs-gluon coupling*, *Phys.Rev.* **D88** (2013) 074015, [[arXiv:1308.2225](#)].
- [28] A. Banfi, A. Martin, and V. Sanz, *Probing top-partners in Higgs+jets*, *JHEP* **1408** (2014) 053, [[arXiv:1308.4771](#)].
- [29] T. Corbett, O. Eboli, J. Gonzalez-Fraile, and M. Gonzalez-Garcia, *Determining Triple Gauge Boson Couplings from Higgs Data*, *Phys.Rev.Lett.* **111** (2013), no. 1 011801, [[arXiv:1304.1151](#)].
- [30] A. Azatov and A. Paul, *Probing Higgs couplings with high  $p_T$  Higgs production*, *JHEP* **1401** (2014) 014, [[arXiv:1309.5273](#)].
- [31] C. Grojean, E. Salvioni, M. Schlaffer, and A. Weiler, *Very boosted Higgs in gluon fusion*, *JHEP* **1405** (2014) 022, [[arXiv:1312.3317](#)].
- [32] C. Anders, C. Bernaciak, G. Kasieczka, T. Plehn, and T. Schell, *Benchmarking an Even Better HEPTopTagger*, *Phys.Rev.* **D89** (2014) 074047, [[arXiv:1312.1504](#)].
- [33] T. Plehn, P. Schichtel, and D. Wiegand, *MadMax, or Where Boosted Significances Come From*, [arXiv:1311.2591](#).

- [34] C. Englert, M. McCullough, and M. Spannowsky, *Gluon-initiated associated production boosts Higgs physics*, *Phys.Rev.* **D89** (2014), no. 1 013013, [arXiv:1310.4828].
- [35] D. E. Ferreira de Lima, A. Papaefstathiou, and M. Spannowsky, *Standard model Higgs boson pair production in the  $(b\bar{b})(b\bar{b})$  final state*, *JHEP* **1408** (2014) 030, [arXiv:1404.7139].
- [36] G. Belanger, V. Bizouard, and G. Chalons, *Boosting Higgs decays into gamma and a Z in the NMSSM*, *Phys.Rev.* **D89** (2014) 095023, [arXiv:1402.3522].
- [37] J. Bramante, A. Delgado, and A. Martin, *Cornering a Hyper Higgs: Angular Kinematics for Boosted Higgs Bosons with Top Pairs*, *Phys.Rev.* **D89** (2014) 093006, [arXiv:1402.5985].
- [38] M. Schlaffer, M. Spannowsky, M. Takeuchi, A. Weiler, and C. Wymant, *Boosted Higgs Shapes*, arXiv:1405.4295.
- [39] M. B. Einhorn and J. Wudka, *Higgs-Boson Couplings Beyond the Standard Model*, *Nucl.Phys.* **B877** (2013) 792–806, [arXiv:1308.2255].
- [40] J. Ellis, V. Sanz, and T. You, *Complete Higgs Sector Constraints on Dimension-6 Operators*, *JHEP* **1407** (2014) 036, [arXiv:1404.3667].
- [41] J. Brod, U. Haisch, and J. Zupan, *Constraints on CP-violating Higgs couplings to the third generation*, *JHEP* **1311** (2013) 180, [arXiv:1310.1385].
- [42] G. Bevilacqua and M. Worek, *On the ratio of  $t\bar{t}b\bar{b}$  and  $t\bar{t}j\bar{j}$  cross sections at the CERN Large Hadron Collider*, *JHEP* **1407** (2014) 135, [arXiv:1403.2046].
- [43] S. Khatibi and M. M. Najafabadi, *Exploring the Anomalous Higgs-top Couplings*, arXiv:1409.6553.
- [44] F. Demartin, F. Maltoni, K. Mawatari, B. Page, and M. Zaro, *Higgs characterisation at NLO in QCD: CP properties of the top-quark Yukawa interaction*, *Eur.Phys.J.* **C74** (2014), no. 9 3065, [arXiv:1407.5089].
- [45] S. Dawson, I. Lewis, and M. Zeng, *Effective Field Theory for Higgs Plus Jet Production*, arXiv:1409.6299.
- [46] M. Wiesemann, R. Frederix, S. Frixione, V. Hirschi, F. Maltoni, et al., *Higgs production in association with bottom quarks*, arXiv:1409.5301.
- [47] G. Isidori, Y. Nir, and G. Perez, *Flavor Physics Constraints for Physics Beyond the Standard Model*, *Ann.Rev.Nucl.Part.Sci.* **60** (2010) 355, [arXiv:1002.0900].
- [48] T. G. Rizzo, *Gluon Final States in Higgs Boson Decay*, *Phys.Rev.* **D22** (1980) 178.
- [49] R. P. Kauffman, S. V. Desai, and D. Risal, *Production of a Higgs boson plus two jets in hadronic collisions*, *Phys.Rev.* **D55** (1997) 4005–4015, [hep-ph/9610541].
- [50] R. P. Kauffman and S. V. Desai, *Production of a Higgs pseudoscalar plus two jets in hadronic collisions*, *Phys.Rev.* **D59** (1999) 057504, [hep-ph/9808286].
- [51] A. Alloul, N. D. Christensen, C. Degrande, C. Duhr, and B. Fuks, *FeynRules 2.0 - A complete toolbox for tree-level phenomenology*, arXiv:1310.1921.
- [52] J. Alwall, R. Frederix, S. Frixione, V. Hirschi, F. Maltoni, et al., *The automated computation of tree-level and next-to-leading order differential cross sections, and their matching to parton shower simulations*, arXiv:1405.0301.
- [53] A. Birkedal, K. Matchev, and M. Perelstein, *Dark matter at colliders: A Model independent approach*, *Phys.Rev.* **D70** (2004) 077701, [hep-ph/0403004].
- [54] M. Beltran, D. Hooper, E. W. Kolb, Z. A. Krusberg, and T. M. Tait, *Maverick dark matter at colliders*, *JHEP* **1009** (2010) 037, [arXiv:1002.4137].
- [55] J. Goodman, M. Ibe, A. Rajaraman, W. Shepherd, T. M. Tait, et al., *Constraints on Dark Matter from Colliders*, *Phys.Rev.* **D82** (2010) 116010, [arXiv:1008.1783].
- [56] Y. Bai, P. J. Fox, and R. Harnik, *The Tevatron at the Frontier of Dark Matter Direct Detection*, *JHEP* **1012** (2010) 048, [arXiv:1005.3797].
- [57] C. Englert and M. Spannowsky, *Effective Theories and Measurements at Colliders*, arXiv:1408.5147.
- [58] **ATLAS Collaboration** Collaboration, G. Aad et al., *Measurement of the  $t\bar{t}$  production cross section in the tau+jets channel using the ATLAS detector*, *Eur.Phys.J.* **C73** (2013) 2328, [arXiv:1211.7205].
- [59] **CMS Collaboration** Collaboration, S. Chatrchyan et al., *Measurement of the  $t\bar{t}$  production cross section in the dilepton channel in pp collisions at  $\sqrt{s} = 8$  TeV*, *JHEP* **1402** (2014) 024, [arXiv:1312.7582].
- [60] **ATLAS Collaboration** Collaboration, G. Aad et al., *Measurement of the  $t\bar{t}$  production cross-section*

- using  $e\mu$  events with  $b$ -tagged jets in  $pp$  collisions at  $\sqrt{s} = 7$  and  $8$  TeV with the ATLAS detector, [arXiv:1406.5375](#).
- [61] **CMS Collaboration** Collaboration, V. Khachatryan et al., *Measurement of top quark-antiquark pair production in association with a  $W$  or  $Z$  boson in  $pp$  collisions at  $\sqrt{s} = 8$  TeV*, [arXiv:1406.7830](#).
  - [62] **CMS Collaboration** Collaboration, *Search for Heavy Resonances Decaying into  $bb$  and  $bg$  Final States in  $pp$  Collisions at  $\sqrt{s} = 8$  TeV*, Tech. Rep. CMS-PAS-EXO-12-023, CERN, Geneva, 2013.
  - [63] **ATLAS Collaboration** Collaboration, G. Aad et al., *Measurement of Higgs boson production in the diphoton decay channel in  $pp$  collisions at center-of-mass energies of 7 and 8 TeV with the ATLAS detector*, [arXiv:1408.7084](#).
  - [64] **CMS Collaboration** Collaboration, V. Khachatryan et al., *Observation of the diphoton decay of the Higgs boson and measurement of its properties*, [arXiv:1407.0558](#).
  - [65] T. Sjostrand, S. Mrenna, and P. Z. Skands, *A Brief Introduction to PYTHIA 8.1*, *Comput.Phys.Commun.* **178** (2008) 852–867, [[arXiv:0710.3820](#)].
  - [66] J. de Favereau, C. Delaere, P. Demin, A. Giammanco, V. Lematre, et al., *DELPHES 3, A modular framework for fast simulation of a generic collider experiment*, [arXiv:1307.6346](#).
  - [67] **CMS Collaboration** Collaboration, S. Chatrchyan et al., *Identification of  $b$ -quark jets with the CMS experiment*, *JINST* **8** (2013) P04013, [[arXiv:1211.4462](#)].
  - [68] D. L. Rainwater, R. Szalapski, and D. Zeppenfeld, *Probing color singlet exchange in  $Z +$  two jet events at the CERN LHC*, *Phys.Rev.* **D54** (1996) 6680–6689, [[hep-ph/9605444](#)].
  - [69] **CMS Collaboration** Collaboration, I. Marfin, *Search for Higgs boson production in association with  $b$  quarks at CMS in  $pp$  collisions*, [arXiv:1301.4412](#).
  - [70] **CMS Collaboration** Collaboration, *Higgs to tau tau (MSSM) (HCP)*, Tech. Rep. CMS-PAS-HIG-12-050, CERN, Geneva, 2012.
  - [71] **ATLAS Collaboration** Collaboration, G. Aad et al., *Search for neutral MSSM Higgs bosons decaying to  $\tau^+\tau^-$  pairs in proton-proton collisions at  $\sqrt{s} = 7$  TeV with the ATLAS detector*, *Phys.Lett.* **B705** (2011) 174–192, [[arXiv:1107.5003](#)].